Nanoscale Res Lett (2010) 5:1195–1203
DOI 10.1007/s11671-010-9626-x

NANO EXPRESS

Binary and Ternary Heterometallic (La^{3+}, Gd^{3+}, Y^{3+})–Eu^{3+} Functionalized SBA-15 Mesoporous Hybrids: Chemically Bonded Assembly and Photoluminescence

Bing Yan · Li-Li Kong

Received: 20 March 2010 / Accepted: 30 April 2010 / Published online: 16 May 2010

Abstract A novel kind of organic–inorganic monomer SUASi has been achieved by modifying 5-sulfosalicylic acid (SUA) with 3-aminopropyltrimethoxysilane (APS), subsequently binary and ternary Eu^{3+} mesoporous hybrid materials with 5-sulfosalicylic acid (SUA)-functionalized SBA-15 and 1,10-phenanthroline (phen) are synthesized by co-condensation of SUASi and TEOS in the presence of Eu^{3+} complex and Pluronic P123 as a template. Finally, luminescent hybrid mesoporous materials consisting of active rare earth ions (Eu^{3+})—inert rare earth ions (Y^{3+}, La^{3+}, Gd^{3+}) complex covalently bonded to the mesoporous materials network have been obtained via this sol–gel approach. The physical characterization and photoluminescence of all these resulting materials are studied in detail. Especially the luminescent behavior has been studied with the different ratios of Eu^{3+}–(Y^{3+}, La^{3+}, Gd^{3+}), which suggests that the existence of inert rare earth ions can enhance the luminescence intensity of Eu^{3+}. This may be due to the intramolecular energy transfer between Y^{3+}, La^{3+}, Gd^{3+}, and Eu^{3+} through the covalently bonded mesoporous framework.

Keywords Heterometallic hybrid mesoporous materials · Rare earth ions · Covalently bonded · Photoluminescence · Energy transfer

B. Yan (✉) · L.-L. Kong
Department of Chemistry, Tongji University, Siping Road 1239, 200092 Shanghai, China
e-mail: byan@tongji.edu.cn

Introduction

Recently, rare earth hybrid inorganic/organic materials have attracted more attention due to their diverse potential applications in catalysis, gas adsorption, magnetism, optical devices or lasers [1–4]. Many rare earth complexes have been investigated thoroughly and applied in the luminescence hybrid materials owing to the long-lived excited-states character and especially the efficient strong narrow-width emission band in the visible region of rare earth ions [5]. Recently, the hybrid material systems of rare earth organic complexes introduced in silica gel have already been found to have superior characteristic emission intensities compared with simple rare earth ions in inorganic hosts. In particular, lots of investigations have been done on the sol–gel-derived host hybrid materials fabricated with rare earth complexes with β-diketones, aromatic, carboxylic acids, and heterocyclic ligands [6]. These studies indicate that the thermal stabilities and mechanical properties of the hybrid materials can be improved by the silica matrices. Our research group has realized some modification path to design functional bridge to further assemble the hybrid materials in which luminescent rare earth complexes species are bonded with siloxane matrix through Si–C linkage [7–9].

Since early 1990s, ordered mesoporous materials with unique properties (high surface area, high pore volume, controlled pore structure, and uniform pore size distribution) are of great interest for adsorption, sensing, catalysis, and other applications [10–13]. Recently, there are some research concerns on the use of ordered mesoporous silica materials as a support for rare earth complexes [14–17]. SBA-15 is a typical mesoporous material with largest pore-size mesochannels, thick walls, adjustable pore size from 3 to 30 nm, and high hydrothermal, thermal, mechanical

stability, so some works have been reported on the hybrids using SBA-15 as host to incorporate active molecules [18–20]. The large number of hydroxyl groups in SBA-15 provides it necessary qualification for the modification of inner face and self-assembly of huge guest molecules, namely, providing outstanding hosts for self-aggregation chemistry. Recently, some work brings out the mesoporous SBA-15 more extensive applications to functionalize its exterior and/or interior surfaces to prepare the organic/inorganic hybrids. Our research team has reported the synthesis and luminescence properties of SBA-15 mesoporous materials covalently bonded with rare earth complexes [21–23].

Some researches have found that the rare earth ions with stable electronic configuration (4f shells are empty, half-filled, and full), such as La^{3+}, Y^{3+}, Gd^{3+}, and Lu^{3+} can enhance the luminescence of photoactive lanthanide ions (Eu^{3+}, Tb^{3+}) [24–26]. But it is hard to clearly prove the luminescent hybrid materials are homogenous at molecular level, so these researches are concentrated on the RE complexes in which luminescence enhancement mainly belongs to intermolecular energy transfer. We have carried some studies on the mechanism of co-luminescence, which is excited by intra-molecular energy transfer [27].

In this paper, we discuss the synthesis of a series of heterometallic hybrid mesoporous materials, in which inert rare earth, such as La^{3+}, Gd^{3+}, Y^{3+}, and the active rare earth ion (Eu^{3+}) are introduced through the covalently bonded SBA-15 framework, and the luminescence enhancement can be found through the intramolecular energy transfer within the hybrid mesoporous materials system.

Experimental Section

Chemicals

Starting materials are purchased from Aldrich and are used as received. All organic solvents are distilled before utilization according to the literature procedures. Rare earth nitrates are obtained by dissolving their oxides in concentrated nitric acid (HNO_3).

Synthesis of the Precursor SUASi from the Modification of 5-Sulfosalicylic Acid

The functional precursor SUASi is prepared according to the procedure reported in the literature [28] (see Fig. 1). First, 5-sulfosalicylic acid is converted to sulfonic chloride: 5-Sulfosalicylic acid (1 mmol, 0.254 g) is dissolved in 20 ml N, N-dimethylformamide (DMF) and then $SOCl_2$ (1 mmol, 0.119 g) is added to the solution drop by drop. The mixed solution is refluxing at 120°C for 4 h. After isolation, the residue is recrystallized by toluene. Then a yellow solid powder is obtained, which is 5-sulfosalicylic sulfonic chloride (SUCl). 5-SUCl can directly react with 3-aminopropyltrimethoxysilane (APS) in DMF to synthesize the sulfonamide linkage: 1 mmol sulfonic chloride is dissolved in DMF by stirring and 1 mmol APS is then added to the solution by drops. The whole mixture is refluxing at 80°C for 4 h. After isolation, a red oil product is obtained, named as SUASi. $C_{25}H_{27}O_8SSi$: ^{1}HNMR 7.99 (1H, s), 3.56 (6H, q), 2.98 (9H, t), 2.86(6H, m), 2.69(3H, s), 1.68 (1H, s), 0.66 (1H, s).

Synthesis of SUA-Functionalized SBA-15 Mesoporous Material

The mesoporous material SUASi-SBA-15 is synthesized from acidic mixture with the following molar composition: 0.0172P123: 0.96TEOS: 0.04SUASi: 6HCl: 208.33H_2O. P123 (1.0 g) is first dissolved in the deionized water (7.5 g) and 2 M HCl solution (30 g) at room temperature. After that the mixture of SUASi and TEOS is added into the above solution followed by 24 h of persistent stirring. Then it is heated at 100°C for 48 h in a Teflon bottle sealed in an autoclave. The solid product is filtered, washed thoroughly with deionized water, and dried at 60°C. The copolymer surfactant P123 is removed via Soxhlet extraction with ethanol under reflux for 2 days. After dried in vacuum, the material showed a light-yellow color (denoted as SUASi-SBA-15).

Synthesis of Hybrid Materials

The sol–gel-derived hybrid materials are prepared according to the similar method in ref. [28], denoted as Eu-SUASi and Eu-SUASi-phen. For binary hybrid mesoporous material: SUASi-SBA-15 is soaked in an appropriate amount of $Eu(NO_3)_3$ ethanol solution with stirring, the molar ratio of Eu^{3+}:SUASi is 1:3. After being stirred for 12 h at room temperature, the mixture is filtrated and washed with ethanol solvent. Finally, the material is dried at 60°C under vacuum overnight, denoted as Eu-SUASi-SBA-15. For ternary hybrid mesoporous material: the synthesis procedure for phen-Eu-SUASi-SBA-15 is similar to the above except that the mixed ethanol solution of $Eu(NO_3)_3$ and 1,10-phenanthroline (phen) replace $Eu(NO_3)_3$, and the molar ratio of Eu^{3+}:SUASi:phen is 1:3:1. The predicted structure of phen-Eu-SUASi-SBA-15 is shown in Fig. 1. The modified ligand is covalently bonded to the SBA-15 host through Si–O-Si by the hydrolysis-condensation of SUASi, denoted as phen-Eu-SUASi-SBA-15. Using the same method, we also have prepare active rare earth ions (Eu^{3+}) and inert rare earth

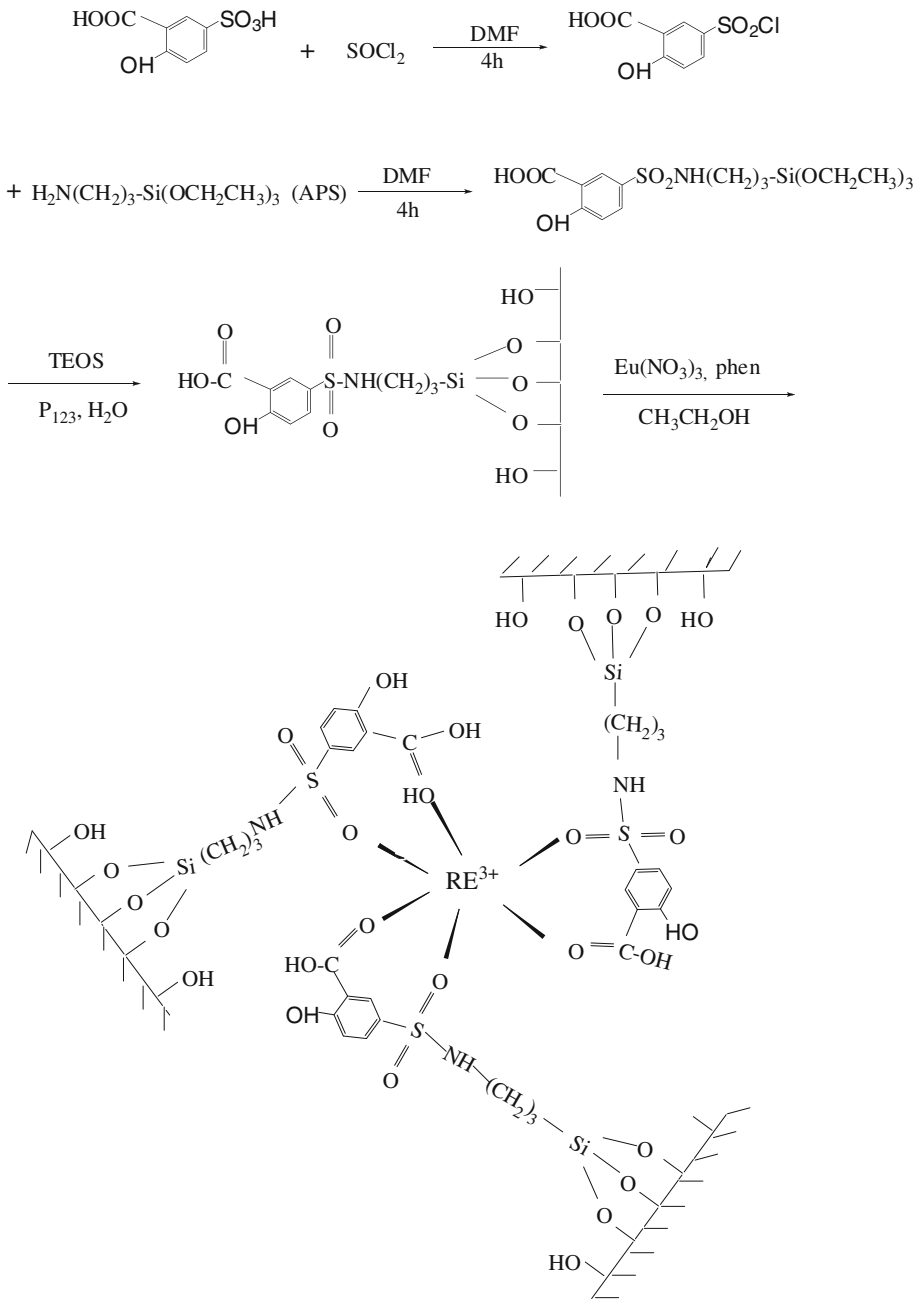

Fig. 1 The scheme for the synthesis process of SUASi and the selected hybrid mesoporous material phen-Eu-SUASi-SBA-15

ions (La^{3+}, Gd^{3+}, Y^{3+}) heterometallic hybrid materials with the different molar ratio (Eu^{3+}:La^{3+} = 5:5; Eu^{3+}:Gd^{3+} = 5:5; Eu^{3+}:Y^{3+} = 1:9, 2:8, 3:7, 4:6, 5:5, 6:4, 7:3, 8:2, 9:1).

Characterization

^{1}H NMR spectra are recorded on a BRUKER AVANCE-500 spectrometer with tetramethylsilane (TMS) as internal reference using $CDCl_3$ as solvent. IR spectra are measured within the 4000–400 cm^{-1} region on an infrared spectrophotometer with the KBr pellet technique. The ultraviolet absorption spectra are taken with an Agilent 8453 spectrophotometer (CCl_4 solution). X-ray powder diffraction patterns are recorded on a Rigaku D/max-rB diffractometer equipped with a Cu anode in a 2θ range from 0.6° to 6°. Nitrogen adsorption/desorption isotherms are measured at the liquid nitrogen temperature, using a Nova 1000 analyzer. Before the measurements, the samples are outgassed for 2 h in the degas port of the adsorption apparatus at 423 K. Surface areas are calculated by the Brunauer-Emmett-Teller (BET) method and pore size distributions are evaluated from the desorption branches of the nitrogen isotherms using the Barrett-Joyner-Halenda (BJH) model.

Thermogravimetric analysis (TGA) is performed on a Netzsch STA 409 at a heating rate of 15°C/min under nitrogen atmosphere. The luminescence excitation and emission spectra are obtained on RF-5301 spectrophotometer. All spectra are normalized to a constant intensity at the maximum. Luminescence lifetime measurements are carried out on an Edinburgh FLS920 phosphorimeter using a 450 w xenon lamp as excitation source.

Results and discussion

Figure 2 shows the ultraviolet–visible absorption spectra of SUCl and SUASi. From the spectra, it can be easily seen a blue-shift (A → B) due to the major $\pi \rightarrow \pi^*$ electronic transition (from 309 to 301 nm), indicating the modification of the conjugate system. The grafting of the APS, from $-SO_2Cl-$ to $-SO_2NH-$, changed the conjugated system. This leads to the decrease in conjugated degree and increase in transition energy gap because the non-covalent electrons of N atom are less than that of Cl atom [28].

The IR spectra of SUCl and SUASi are shown in Fig. 3a, which presents the similar character to the result in ref. [28]. The ν_{as} (O=S=O) and ν_s (O=S=O) absorption bands located at 1394 and 1254 cm^{-1} can be easily found from the curve of SUCl. The ν (C=O) vibration is observed at 1660 cm^{-1} due to the existence of –COOH. In the curve of SUASi, the grafting reaction is evidenced by the sharp band located at 1246 cm^{-1} according to the ν (S–N). Besides, the ν ($-CH_2-$) located at 2936, 2870 cm^{-1} and the ν (Si–O–C) located at 1101 cm^{-1} further prove the success of the completion reaction. The bands located at 1380 cm^{-1} consisting of the ν (O=S=O) is obviously observed in the curve of the SUASi. The wide absorption band at around 1101 cm^{-1} indicates the dominating of O–Si–O bonds.

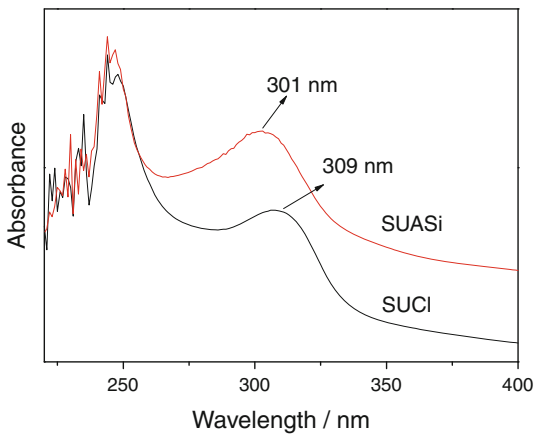

Fig. 2 The ultraviolet–visible absorption spectra of sulfonic chloride and sulfonamide precursor SUASi

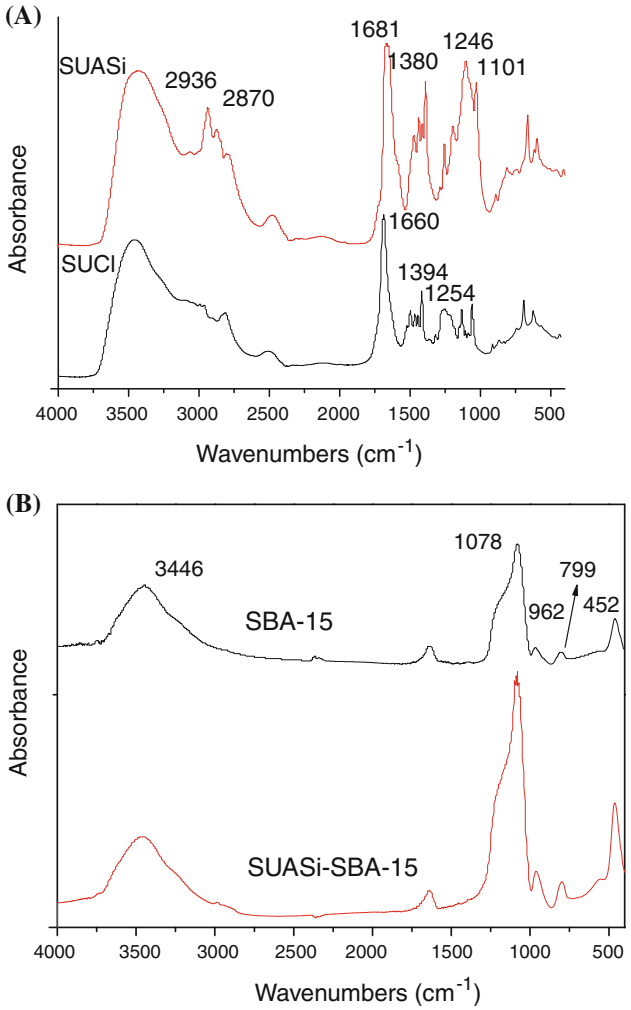

Fig. 3 The IR spectra for precursors **a** SUCl and SUASi; hybrids **b** SBA-15 and SUASi-SBA-15

The IR spectra of SBA-15 and SUASi-SBA-15 are shown in Fig. 3b. In the spectrum of SBA-15 material, the bands at 1078 cm^{-1} and 799 cm^{-1} corresponded to the asymmetric Si–O stretching vibration modes (ν_{as}, Si–O) and the symmetric Si–O stretching vibration (ν_s, Si–O), respectively. The bands at 452 $cm^{-1}$and 962 cm^{-1} are assigned to be the Si–O–Si bending vibration (δ, Si–O–Si) and the silanol (Si–OH) stretching vibrations of surface groups [29]. The band appearing at 3449 cm^{-1} is the evidence of the presence of hydroxyl group. The spectrum of the SUASi-SBA-15 exhibits the parallel infrared absorption bands, proving the successful formation of the silica framework.

SBA-15 is a kind of highly ordered mesoporous material with hexagonal symmetry of the space group p6 mm. These characters can be proved by the small-angle X-ray diffraction (SAXRD) patterns and nitrogen adsorption/desorption isotherms. Figure 4 is the SAXRD patterns of SUASi-SBA-15, Eu-SUASi-SBA-15 and phen-Eu-SUASi-SBA-15.

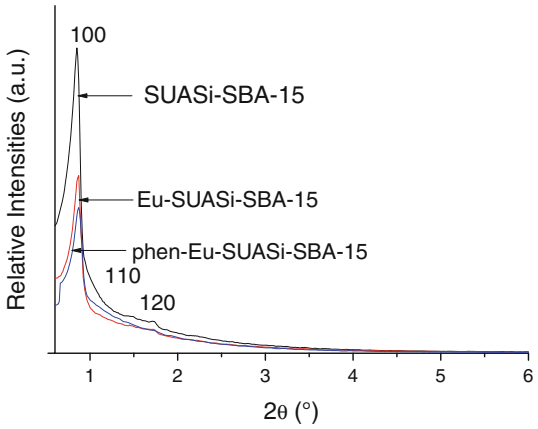

Fig. 4 The SAXRD patterns of the hybrid mesporous materials: SUASi-SBA-15, Eu-SUASi-SBA-15 and phen-Eu-SUASi-SBA-15

All the materials exhibit the well-resolved diffraction peaks that can be indexed to be (100) (110), and (200) diffractions associated with 2-D hexagonal symmetry (*p6mm*). This phenomenon shows the existing of the well-ordered mesoporous structure in these samples. It is also observed that the relative intensity of these characteristic diffraction peaks decreases slightly in all these functionalized mesoporous materials compared with pure SBA-15. The reduction in diffraction intensity can be partly assigned to the presence of guest moieties onto the mesoporous framework of SBA-15 and may also be partly due to the decrease in the mesoscopic order of the materials [30–32]. The presence of guest moieties results in the decrease in crystallinity, but the pore structure of mesoporous materials still exists [33, 34]. Compared with the SAXRD pattern of pure SBA-15, the d_{100} spacing values of SUASi-SBA-15, Eu-SUASi-SBA-15 and phen-Eu-SUASi-SBA-15 are nearly unchanged (see Table 1), suggesting that the ordered hexagonal mesoporous structure of SBA-15 retains intact after both SUA-functionalized and the introduction of Eu^{3+} [21].

Figure 5 displays the N_2 adsorption/desorption isotherms for the hybrid mesoporous materials SUASi-SBA-15, Eu-SUASi-SBA-15 and phen-Eu-SUASi-SBA-15. They all exhibit the type IV isotherms with a clear H1-type hysteresis loop at high relative pressure [35–37], which is related to the capillary condensation of nitrogen within the pores. This is characteristic of highly ordered mesoporous materials according to the IUPAC classification [38]. From the two branches of adsorption–desorption isotherms, both sharp adsorption step in the P/P_0 region from 0.6 to 0.8 and the hysteresis loop at the relative pressure $P/P_0 > 0.5$ show that the hybrid materials possess a well-defined array with regular mesopores. The specific area and the pore size have been calculated by using Brunauer-Emmett-Teller (BET) and Barrett-Joyner-Halenda (BJH) methods, respectively. And the structure data of all these mesoporous materials (BET surface area, total pore volume, and pore size, etc.) are summarized in Table 1. From Table 1, it can be conclude that the SUASi-SBA-15 exhibits a smaller specific area and a slightly smaller pore size and pore volume in comparison with those of pure SBA-15, which might be due to the presence of organic ligand SUA on the pore surface and the co-surfactant effect of SUASi, which interacts with surfactant and reduces the diameter of the micelles. In addition, after introducing Eu^{3+} into the SUASi-SBA-15, the specific area, pore size, and pore volume of the Eu^{3+} containing materials are less than those of SUASi-SBA-15. This phenomenon can also prove that the Eu^{3+} complexes have been incorporated into the channels of SBA-15.

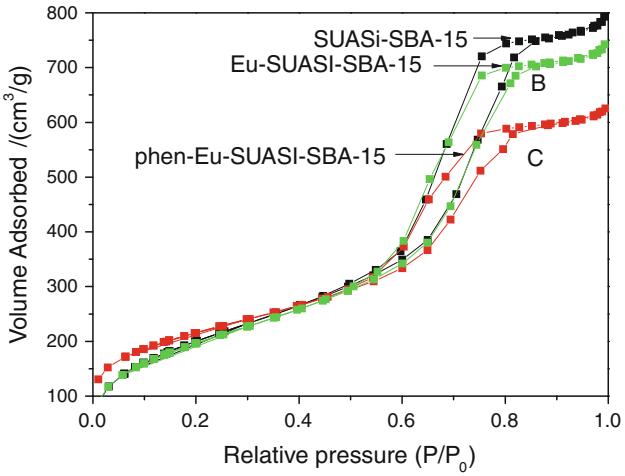

Fig. 5 The N_2 adsorption/desorption isotherms for SUASi-SBA-15, Eu-SUASi-SBA-15 and phen-Eu-SUASi-SBA-15

Table 1 Textural data of hybrid mesoporous materials SUASi-SBA-15, Eu-SUASi-SBA-15 and phen-Eu-SUASi-SBA-15 materials

Sample	D_{100} (nm)	S_{BET} (m^2/g)	V (cm^3/g)	D_{BJH} (nm)	a_0	t
SUA-SBA-15	10.39	742	1.22	5.86	11.99	6.13
Eu-SUASi-SBA-15	10.15	701	1.13	5.69	11.72	6.03
phen-Eu-SUASi-SBA-15	10.13	576	0.87	5.47	11.69	6.22

d_{100} is the $d(100)$ spacing ($2d\sin\theta = n\lambda$, $\lambda = 154.18$ pm), a_0 is the cell parameter ($a_0 = 2d_{100}/\sqrt{3}$), S_{BET} is the BET surface area, V is the pore volume, D is the pore diameter, and t is the wall thickness, calculated by a_0-D

The thermogravimetric weight loss (TG) curve of the ternary complex phen-Eu-SUASi and ternary hybrid mesoporous material phen-Eu-SUASi-SBA-15 is given in Fig. 6. It can be observed that the mesoporous materials have remained the more residual mass (67%) compared to the hybrid materials (20%). Furthermore, the TGA curve of mesoporous materials has one decomposition platform while the hybrid materials has two decomposition stages, indicating that the mesoporous materials is more stable for thermal treatment compared to the pure complex. Besides, the mass change of the mesoporous materials begins at 150°C while the hybrid materials started at 100°C. In conclusion, the mesoporous materials have better thermal stability compared with the hybrid materials. It can be explained that the thermal stability of the organic compounds has increased when it is covalently bonded to the mesoporous matrix.

The luminescence spectra of the all the prepared materials have been measured at room temperature. Figure 7 shows the excitation and emission spectra for the hybrid mesoporous materials Eu-SUASi-SBA-15 (A) and phen-Eu-SUASi-SBA-15 (B). The excitation spectra of these materials at room temperature are all obtained by monitoring the strongest emission wavelength of the Eu^{3+} ions at 613 nm. Only the emission spectrum of the hybrid materials phen-Eu-SUASi-SBA-15 exhibits the emission consisting of the $^5D_0 \rightarrow {}^7F_1$, $^5D_0 \rightarrow {}^7F_2$, $^5D_0 \rightarrow {}^7F_3$ and $^5D_0 \rightarrow {}^7F_4$ transitions at 588, 614, 649, and 700 nm, respectively. These phenomena suggest that the introduction of phen may have apparent influence on the luminescent property within the hybrid systems. In addition, the relative intensities ration (I_{02}/I_{01}) of the hybrid mesoporous material phen-Eu-SUASi-SBA-15 is higher than the non-mesporous hybrid material Eu-SUASi-phen (see Table 2), indicating that the luminescence properties of the mesoporous material can be improved after the introduction of the ligand into the mesoporous matrix.

The luminescence spectra for the homometallic and heterometallic hybrid mesoporous materials are shown in Fig. 8a. All the emission peaks of the hybrid mesoporous materials are assigned to the characteristic $^5D_0 \rightarrow {}^7F_1$ and $^5D_0 \rightarrow {}^7F_2$ transitions of Eu^{3+} at 588 and 614 nm while the emission lines of $^5D_0 \rightarrow {}^7F_3$ and $^5D_0 \rightarrow {}^7F_4$ are weak except in the spectra of Y^{3+}–Eu^{3+} (D) heterometallic hybrid mesoporous materials. Besides, the relative intensities ration (I_{02}/I_{01}) is enhanced after the introduction of the inert rare earth ions (see Table 2). This can be concluded that SUA can sensitize active rare earth ions Eu^{3+}, and the hybrid mesoporous materials have better luminescence properties. The luminescence intensities of mesoporous hybrid materials have been improved with the co-fabrication of inert rare earth ions because the

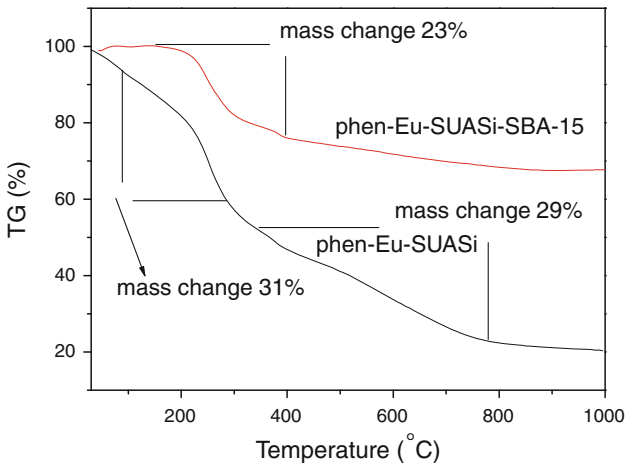

Fig. 6 The selected thermogravimetric weight loss curve (TG) of phen-Eu-SUASi and phen-Eu-SUASi-SBA-15

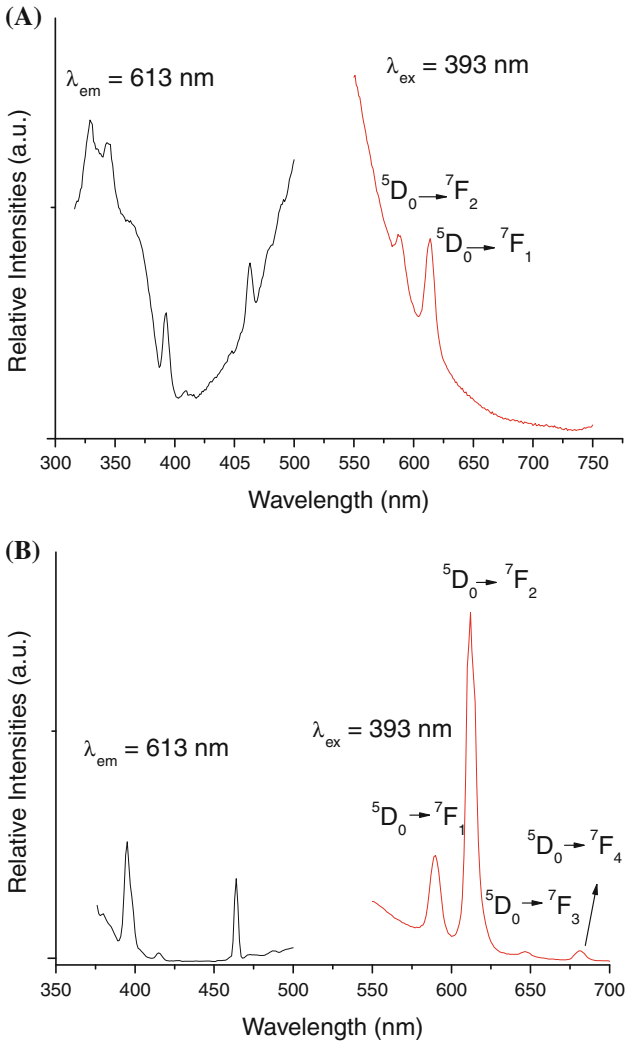

Fig. 7 The excitation and emission spectra for the binary and ternary hybrid mesoporous materials Eu-SUASi-SBA-15 (**a**) and phen-Eu-SUASi-SBA-15 (**b**)

Table 2 Photoluminescent data of the selected ternary homometallic and heterometallic hybrid mesoporous hybrid materials

Systems	phen-Eu-SUASi	phen-Eu-SUASi-SBA-15	phen-La-Eu-SUASi-SBA-15	phen-Gd–Eu-SUASi-SBA-15	phen-Y-Eu-SUASi-SBA-15
τ (ms)	0.213	0.295	0.294	0.283	0.345
I_{02}/I_{01}	1.86	3.39	4.32	5.05	6.00
A_{01} (s^{-1})	50	50	50	50	50
A_{02} (s^{-1})	97.5	176.0	225.0	262.6	312.6
A_{03} (s^{-1})	5.7	0.07	0.05	0	6.7
A_{04} (s^{-1})	6.4	0.08	0.05	0	9.7
A_{rad} (s^{-1})	159.6	226.2	275.1	312.6	379.0
η (%)	3.4	6.7	8.1	8.9	13.0

luminescence enhancement effect occurs. And we also find the Y^{3+}–Eu^{3+} heterometallic hybrid mesoporous materials have more advantages than others.

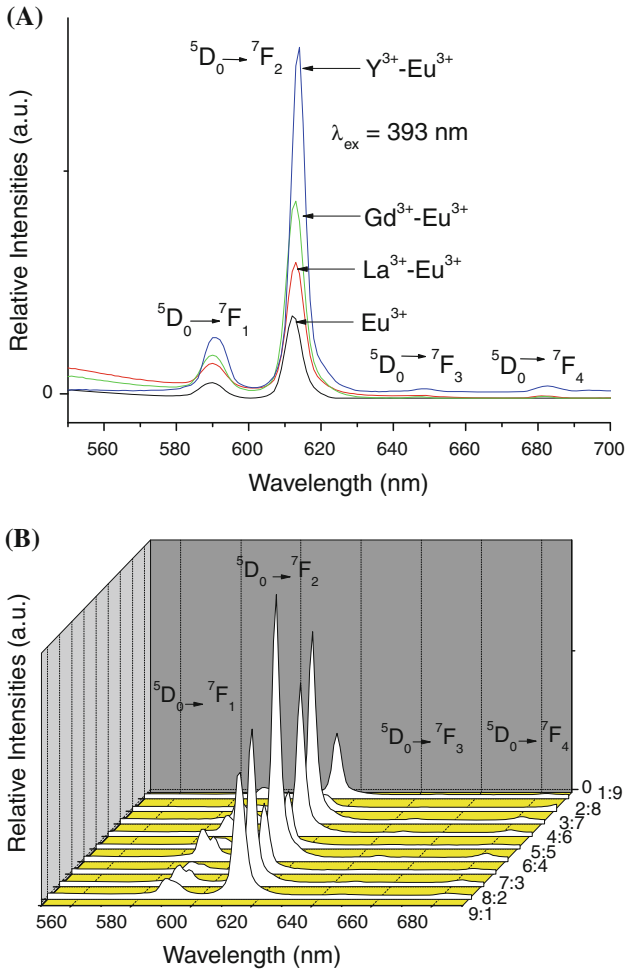

Fig. 8 The comparison of emission spectra for the hybrid mesoporous materials with different rare earth ions (**a**): Eu^{3+}, La^{3+}–Eu^{3+}, Gd^{3+}–Eu^{3+}, Y^{3+}–Eu^{3+}; and the comparison of emission spectra for the Y^{3+}–Eu^{3+} heterometallic hybrid mesoporous materials with different molar ratio of Y^{3+}:Eu^{3+}: 1:9, 2:8, 3:7, 4:6, 5:5, 6:4, 7:3, 8:2, 9:1 (**b**)

Further, we compare the emission spectra for the Y^{3+}–Eu^{3+} heterometallic hybrid mesoporous materials with different molar ratio of Y^{3+}:Eu^{3+} (1:9, 2:8, 3:7, 4:6, 5:5, 6:4, 7:3, 8:2, 9:1) is shown in Fig. 8b. All the hybrid mesoporous materials exhibit the characteristic emission lines of Eu^{3+}. From the emission spectrum, when the molar ratio Y^{3+}:Eu^{3+} = 4:6, the intensity of the spectrum is stronger than others. This is the best proportion for Y^{3+}–Eu^{3+} heterometallic hybrid mesoporous materials with the best luminescent intensities.

The typical decay curves of these prepared materials have been measured and they can be described as a single exponential ($\mathrm{Ln}(S(t)/S0) = -kt = -t/\tau$), indicating that all Eu^{3+} ions occupy the same average coordination environment. According to the emission spectrum and the lifetime of the Eu^{3+} first excited level (τ, $^5D_0$), the emission quantum efficiency (η) of the $^5D_0$ Eu^{3+} excited state can be determined. Assuming that only non-radiative and radiative processes are essentially involved in the depopulation of the $^5D_0$ state, η can be defined as follows [39–43]:

$$\eta = \frac{A_r}{A_r + A_{nr}} \quad (1)$$

where A_r and A_{nr} are radiative and non-radiative transition rates, respectively. A_r can also be obtained by summing over the radiative rates A_{0J} for each $^5D_0 \rightarrow {}^7F_J$ (J = 0–4) transitions of Eu^{3+}. The quantum efficiency data are shown in Table 2. From the equation of η, it can be seen the η value mainly depends on the values of lifetimes and I_{02}/I_{01}. As can be seen from Table 2, the quantum efficiency of phen-Eu-SUASi-SBA-15 (6.7%) is higher than that of phen-Eu-SUASi (3.4%), which can be ascribed to the substitution of the silanol with covalently bonded SUA groups in the pore channel of mesoporous SBA-15, resulted in the decrease in the level of non-radiative multiphonon relaxation by coupling to –OH vibrations and non-radiative transition rate. This clearly demonstrates the modifications in the Eu^{3+} ion local environment as

phen-Eu-SUASi is covalently bonded to the mesoporous SBA-15. The results described above further provide the indirect formation on that phen-Eu-SUASi is successfully covalently bonded to the SBA-15 network. Furthermore, the quantum efficiencies of the heterometallic hybrid mesoporous materials have been increased, and among them the Y^{3+}–Eu^{3+} heterometallic hybrid mesoporous materials have the maximum quantum efficiency compared with others. This phenomenon is another evidence for that the energy transfer efficient from the ligand to the Eu^{3+} is improved when the inert rare earth ions are introduced.

From the above results, we give the primary analyses on the luminescent enhancement. For the heterometallic covalently bonded hybrid mesoporous system, Eu^{3+} and inert rare earth ions (La^{3+}, Gd^{3+}, Y^{3+}) coexist in the same huge molecular hybrids through the covalently bonded SBA-15 ordered Si–O framework. So it can be predicted that the intramolecular energy transfer process from the energy donor (SUASi-SBA-15) to Eu^{3+} can be enhanced for the inert RE^{3+} can strengthen the excitation of organic ligand unit, which take agreement with the similar phenomenon in other systems [20, 23]. But the proportion of inert ion exceeds one optimum value, as the concentration of inert RE^{3+} increase further, active luminescent center (Eu^{3+}) reduces and the luminescence intensity of the system wanes.

Conclusion

In summary, we have assembled the luminescent organic–inorganic hybrid mesoporous materials by linking homometallic and heterometallic rare earth complexes (Eu^{3+}, La^{3+}–Eu^{3+}, Gd^{3+}–Eu^{3+}, Y^{3+}–Eu^{3+}) to the functionalized ordered mesoporous SBA-15 through the modified SUASi bridge via co-condensation of TEOS in the presence of Pluronic P123 surfactant as a template. The luminescent behavior has been studied with the different ratios of active rare earth ions (Eu^{3+}) and inert rare earth ions (La^{3+}, Y^{3+}, Gd^{3+}), which suggests that the existence of inert rare earth ions can enhance the luminescence behavior (luminescent intensity, lifetime, and quantum yields), which may be due to the intramolecular energy transfer between inert rare earth ions and active rare earth ions. Among them Y^{3+}:Eu^{3+} = 4:6 is the best ratio for Y^{3+}–Eu^{3+} heterometallic hybrid mesoporous materials with the optimum luminescence property. Their luminescent property, thermal stability, highly ordered hexagonal channel structure and uniform pore sizes of the organic group functionalized SBA-15 mesoporous materials will be expected to expand their applications in both optical and electrical molecular devices.

Acknowledgments This work is supported by the National Natural Science Foundation of China (20971100) and Program for New Century Excellent Talents in University (NCET-08-0398).

References

1. A.A. Adjei, Invest. New Drugs. **17**, 43 (1999)
2. A. Clearfield, Curr. Opin. Solid State Mater. Sci. **1**, 268 (1996)
3. L.D. Carlos, R.A.S. Ferreira, V.D. Bermudez, J.L.S. Ribeiro, Adv. Mater. **21**, 509 (2009)
4. K. Binnemans, Chem. Rev. **109**, 4283 (2009)
5. L.R. Matthews, E.T. Knobbe, Chem. Mater. **5**, 1697 (1993)
6. P.A. Tanner, B. Yan, H.J. Zhang, J. Mater. Sci. **35**, 4325 (2000)
7. B. Yan, H.F. Lu, Inorg. Chem. **47**, 5601 (2008)
8. J.L. Liu, B. Yan, J. Phys. Chem. B **112**, 10898 (2008)
9. J.L. Liu, B. Yan, J. Phys. Chem. C **112**, 14168 (2008)
10. D.E. De Vos, M. Dams, B.F. Sels, P.A. Jacobs, Chem. Rev. **102**, 3615 (2002)
11. M.E. Davis, Nature **417**, 813 (2002)
12. A.P. Wight, M.E. Davis, Design and preparation of organic-inorganic hybrid catalysts. Chem. Rev. **102**, 3589–3614 (2002)
13. A. Stein, Adv. Mater. **15**, 763 (2003)
14. Q.H. Xu, L.S. Li, X.S. Liu, R.R. Xu, Chem. Mater. **14**, 549 (2002)
15. M.H. Bartl, B.J. Scott, H.C. Huang, G. Wirnsberger, A. Popitsch, B.F. Chmelka, G.D. Stucky, Chem. Commun. **21**, 2474 (2002)
16. Q.H. Xu, W.J. Dong, H.W. Li, L.S. Li, S.H. Feng, R.R. Xu, Solid State Sci. **5**, 777 (2003)
17. Q.G. Meng, P. Boutinaud, A.C. Franville, H.J. Zhang, R. Mahiou, Microp. Mesop. Mater. **65**, 127 (2003)
18. D.Y. Zhao, J.Y. Sun, Q.Z. Li, G.D. Stucky, Chem. Mater. **12**, 275 (2000)
19. S. Madhugiri, A. Dalton, J. Gutierrez, J.P. Ferraris, K.J. Balkus, J. Am. Chem. Soc. **125**, 14531 (2003)
20. B.J. Scott, G. Wirnsberger, G.D. Stucky, Chem. Mater. **13**, 3140 (2001)
21. Y. Li, B. Yan, H. Yang, J. Phys. Chem. C **112**, 3959 (2008)
22. L.L. Kong, B. Yan, Y. Li, J. Solid State Chem. **182**, 1631 (2009)
23. B. Yan, B. Zhou, J. Photochem. Photobiol. A Chem. **195**, 314 (2008)
24. Y.T. Yang, S.Y. Zhang, Q.D. Su, Mater. Res. Bull. **40**, 1010 (2005)
25. Y. Li, Y.L. Zhao, J. Fluoresc. **19**, 641 (2009)
26. L.M. Zhao, B. Yan, J. Lumin. **118**, 317 (2006)
27. F.F. Wang, B. Yan, J. Photochem. Photobiol. A Chem. **194**, 238 (2008)
28. K. Qian, B. Yan, Polyhedron **29**, 226 (2010)
29. M.V. Landau, S.P. Parkey, M. Herskowitz, O. Regev, S. Pevzner, T. Sen, Z. Luz, Microp. Mesop. Mater. **33**, 149 (1999)
30. M.H. Lim, A. Stein, Chem. Mater. **11**, 3285 (1999)
31. R. Huq, L. Mercier, Chem. Mater. **13**, 4512 (2001)
32. L. Mercier, T.J. Pinnavaia, Chem. Mater. **12**, 188 (2000)
33. L.N. Sun, J.B. Yu, H.J. Zhang, Q.G. Meng, E. Ma, C.Y. Peng, K.Y. Yang, NMicropor. Mesopor. Mater. **98**, 156 (2007)
34. L. Mercier, T.J. Pinnavaia, Adv. Mater. **9**, 500 (1997)
35. K.S.W. Sing, D.H. Everett, R.A.W. Haul, L. Moscou, R.A. Pierotti, J. Rouquerol, T. Siemieniewska, Pure Appl. Chem. **57**, 603 (1985)
36. M. Kruk, M. Jaroniec, Chem. Mater. **13**, 3169 (2001)
37. W.H. Zhang, X.B. Lu, J.H. Xiu, Z.L. Hua, L.X. Zhang, M. Robertson, J.L. Shi, D.S. Yan, J.D. Holmes, Adv. Funct. Mater. **14**, 544 (2004)
38. D.H. Everett, Pure Appl. Chem. **31**, 577 (1972)

39. P.C.R. Soares-Santos, H.I.S. Nogueira, V. Félix, M.G.B. Drew, R.A.S. Ferreira, L.D. Carlos, T. Trindade, Chem. Mater. **15**, 100 (2003)
40. E.S. Teotonio, J.G.P. Espínola, H.F. Brito, O.L. Malta, S.F. Oliveria, D.L.A. de Foria, C.M.S. Izumi, Polyhedron **21**, 1837 (2002)
41. L.D. Carlos, Y. Messaddeq, H.F. Brito, R.A.S. Ferreira, V.D. Bermudez, S.J.L. Ribeiro, Adv. Mater. **12**, 594 (2000)
42. R.A.S. Ferreira, L.D. Carlos, R.R. Gonçalves, S.J.L. Ribeiro, V.D. Bermudez, Chem. Mater. **13**, 2991 (2001)
43. M.H.V. Werts, R.T.F. Jukes, J.W. Verhoeven, Phys. Chem. Chem. Phys. **4**, 1542 (2002)